

# Effects of Neutrons and $\gamma$ -Rays on Scintillation Light in SX Diagnostics for LHD Deuterium Plasma Experiments

Takahiro BANDO<sup>1)</sup>, Satoshi OHDACHI<sup>1,2)</sup> and Yasuhiro SUZUKI<sup>1,2)</sup>

<sup>1)</sup>*SOKENDAI (The Graduate University for Advanced Studies), 322-6 Oroshi-cho, Toki 509-5292, Japan*

<sup>2)</sup>*National Institute for Fusion Science, 322-6 Oroshi-cho, Toki 509-5292, Japan*

(Received 30 June 2015 / Accepted 15 October 2015)

In the Large Helical Device (LHD) semiconductor-based detector arrays for soft X-ray (SX) emission have been used for studying MHD instabilities. However, a semiconductor device is expected to be damaged in high neutron flux environments in the coming LHD deuterium plasma experiments. In order to measure an SX in such environments, a CsI:Tl scintillator-based diagnostic is being developed. Though CsI:Tl is sensitive to a neutron and to a gamma-ray, as well, effects on scintillation light can be reduced if very thin CsI:Tl foil (50 micrometers) is used. An SX is converted to visible light by a scintillator and led to optical fibers. The light is transferred away from LHD and detected by a semiconductor detector array set in a neutron and gamma-ray shielding box. Effects by neutrons and gamma-rays on scintillation light are quantitatively estimated based on the deuterium plasma experiment condition of LHD.

© 2015 The Japan Society of Plasma Science and Nuclear Fusion Research

Keywords: CsI:Tl, soft X-ray, diagnostic, LHD, deuterium plasma, neutron, gamma-ray

DOI: 10.1585/pfr.10.1402090

## 1. Introduction

Multi-channel soft X-ray (SX) emission measurement has been used for studying MHD activities in magnetically confined fusion devices. Since SX emission is constant on a flux surface, deformation of the flux surface can be estimated from the fluctuating component of the SX emission. Therefore, this kind of measurement is quite useful for studying spatial structures of MHD instabilities. For this purpose, semiconductor-based detectors have been used in hydrogen plasma experiments in LHD [1]. Plasma experiments using deuterium gas will start in the near future. In the deuterium plasma experiments, two types of D-D reactions can occur with the same probability.



2.45 MeV neutrons and secondary  $\gamma$ -rays, which mainly come from the vacuum vessel, will damage semiconductors. To measure SXs in such high neutron flux environments, we are developing a new type of an SX diagnostic using a scintillator.

In this diagnostic, an SX is converted to visible light by a scintillator. The light is then guided to a remote location and measured there. CsI:Tl, having high conversion efficiency, is used as the scintillator.

CsI:Tl has two advantages compared with other inorganic scintillators, such as NaI:Tl, CsI:Na, and Bi<sub>4</sub>Ge<sub>3</sub>O<sub>12</sub> in high neutron flux environments. First, CsI:Tl is composed of atoms whose mass numbers are high. There-

fore, an elastic collision of a neutron has little effect on scintillation light, as shown in Sec.3.3. Second, the absolute light yield of CsI:Tl is about 8 times that of Bi<sub>4</sub>Ge<sub>3</sub>O<sub>12</sub> [2]. However, there is a disadvantage that CsI:Tl has a much slower decay time of scintillation light than NaI:Tl, CsI:Na, and Bi<sub>4</sub>Ge<sub>3</sub>O<sub>12</sub>. The decay time of CsI:Tl is approximately 3  $\mu$ s [2]. But this is short enough to detect an MHD fluctuation whose typical frequency is lower than 10 kHz.

This type of a scintillator-based system has been used for imaging of SX emission in some magnetically confined devices [3], and is used in LHD experiments, as well [4]. It is reported that this type of diagnostic is working well even in high neutron flux environments of NSTX [5]. Also, it was proposed for SX measurements in burning plasma experiments BPX [6], and its applicability for BPX was discussed in Ref. [7].

In deuterium plasma experiments, neutrons produce various radiations. These radiations as well as neutrons enter into scintillators and affect scintillation light. To have a scintillator-based SX diagnostic work well in deuterium plasma experiments, at the very least, it is required that the dominant component of scintillation light comes from SXs and not from other radiations.

In this article, quantitative estimations of radiation effects on scintillation light are discussed in detail. In particular, effects by neutrons which directly enter into a scintillator and  $\gamma$ -rays from the vacuum vessel are described. This article is organized as the following. In Sec. 2, design of a diagnostic and the flux of neutron and  $\gamma$ -ray for estimations are introduced. In Sec. 3, effects on scintillation light

author's e-mail: bando.takahiro@nifs.ac.jp

by neutrons which directly enter into a scintillator, and  $\gamma$ -rays from the vacuum vessel and  $\gamma$ -ray shielding around the scintillator are estimated quantitatively. The summary of estimations of the absorption powers to a CsI:Tl scintillator due to SXs, neutrons, and  $\gamma$ -rays will be shown in Sec. 4.

## 2. The Design of the Scintillator-Based SX Diagnostic and the Flux

The schematic view of the detection system considered in this study is shown in Fig. 1. The detection system is essentially a pinhole camera with a scintillator screen. SXs from a plasma go through the pinhole and then enter a CsI:Tl scintillator. The SXs are converted to visible light (scintillation light) there. The light is converged by lenses and led to optical fibers. Then the light is transferred and detected by a semiconductor detector array set in a neutron and  $\gamma$ -ray shielding box far from LHD.

The shape of the scintillator is assumed to be a rectangular solid,  $8\text{ mm} \times 8\text{ mm} \times 50\text{ }\mu\text{m}$ .  $S = 8\text{ mm} \times 8\text{ mm} = 6.4 \times 10^{-5}\text{ m}^2$  is the area on which each radiation is assumed to enter perpendicularly. The thickness of the scintillator  $l$  is  $50\text{ }\mu\text{m}$ . The volume of the scintillator  $V$  is  $3.2 \times 10^{-9}\text{ m}^3$ .

The energy spectrum of the neutron flux and the  $\gamma$ -ray flux, at the place where the scintillator is planned to be set, were calculated with a transport code, DORT [8]. DORT is a transport code which determines the flux or fluence of particles throughout one- or two-dimensional geometric systems due to sources generated as a result of particle interaction with the medium or incident on the system from extraneous sources.

The condition of this DORT calculation is the following. The geometry used in the DORT calculation is shown in Fig. 2. In this figure, each region, denoted by letters, indicates (a) plasma, (b) helical coil, (c) helical coil container, (d) shell support, (e) poloidal coil, (f) vacuum vessel, (g) bell jar, and (h) air. The ion temperature is  $9.46\text{ keV}$  and the line average density is  $2.5 \times 10^{19}\text{ m}^{-3}$ . And, two kinds of NBI are injected. One is a perpendicular injection, which power is  $18\text{ MW}$  and beam energy is  $80\text{ keV}$ . The other is a tangential injection, which power is  $14\text{ MW}$  and beam energy is  $180\text{ keV}$ . Since almost all neutrons

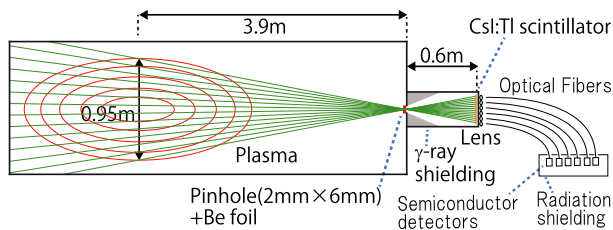


Fig. 1 The schematic view of the detection system is shown. Sight lines viewing a plasma cross section are shown as green lines.

occur by collisions of part of a plasma and energetic particles of the neutral beam, the neutron yield does not much depend on the plasma temperature. The result with this condition shows the maximum neutron yield in deuterium plasma experiments: the  $\gamma$ -ray flux is  $1.06 \times 10^{13}\text{ m}^{-2}\text{ s}^{-1}$ , and the neutron flux is  $4.58 \times 10^{13}\text{ m}^{-2}\text{ s}^{-1}$  at the location of a CsI:Tl scintillator planned to be set in LHD. In estimations in Sec. 3, neutrons and  $\gamma$ -rays are assumed to come from one direction (from the left hand side in Fig. 1) only. In other words, we treat this problem as a one-dimensional problem. It is noted that the result of the DORT calculation does not include information on the direction of the flux. But in reality, neutrons mainly come from the plasma and  $\gamma$ -rays come mainly from the vacuum vessel or other component surrounding the plasma.

A preliminary calculation shows that the effect by  $\gamma$ -rays on scintillation light is as large as the effect by SXs. Therefore, we set stainless steel in front of the scintillator for shielding  $\gamma$ -rays, as shown in Fig. 1. The shape is a column fit in the vacuum chamber with a conical hole for sight lines. The average length of the shielding is  $100\text{ mm}$  when the shielding is seen from a plasma.

The  $\gamma$ -ray shielding can be a source of secondary  $\gamma$ -rays induced by neutrons. The secondary  $\gamma$ -rays from the shielding are calculated by PHITS code ver. 2.76 [9]. PHITS is a Monte Carlo particle transport simulation code used for three-dimensional matter.

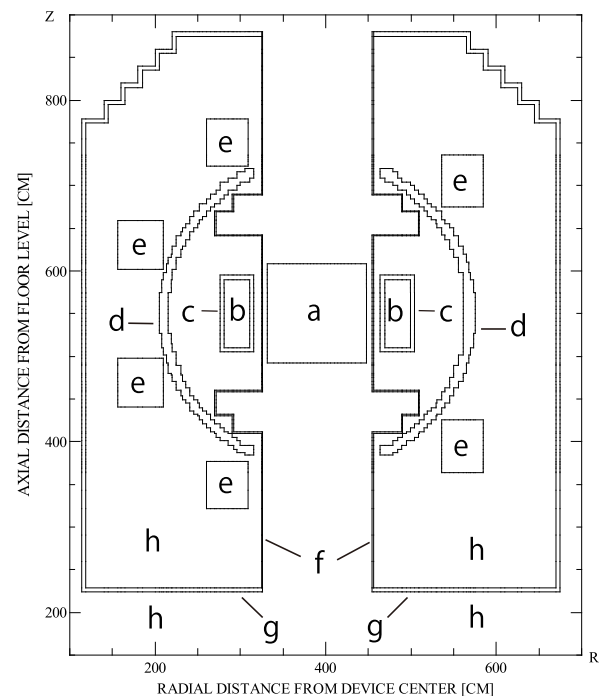


Fig. 2 The geometry used for the DORT calculation. Each region, denoted by letters, indicates (a) plasma, (b) helical coil, (c) helical coil container, (d) shell support, (e) poloidal coil, (f) vacuum vessel, (g) bell jar, and (h) air.

In the PHITS calculation, the shielding shape is assumed to be a cuboid solid, 100 mm on each side. The source of the neutron flux is located in front of the cuboid and 10 mm away from the cuboid. The shape of the source is a plane, 100 mm each side. The direction of the neutron velocity is aligned with the perpendicular line, passing through the center of the plane.

### 3. The Estimation of the Absorption Power to CsI

As mentioned in Sec. 1, to have a scintillator-based diagnostic work well, the dominant component of scintillation light from a scintillator should come from SXs, not from other radiations. In the detector system shown in Fig. 1, neutrons from a plasma, secondary  $\gamma$ -rays from the vacuum vessel, and recoil particles from Be foil or windows will enter into the scintillator and affect the scintillation light. In addition, neutrons which enter into the scintillator produce  $\alpha$  particles and protons, which affect the scintillation light.

In this section, effects on scintillation light by neutrons which directly enter into the scintillator and  $\gamma$ -rays coming from the vacuum vessel are estimated quantitatively with the design shown in Fig. 1. Effect by recoil particles is not considered in this study. This effect is believed to be small based on a simplified estimation using PHITS code.

The amplitude of scintillation light from CsI:Tl is assumed to be proportional to the sum of the absorption power to CsI:Tl. The amount of Tl in CsI is few, thus the power is estimated for only CsI. Therefore, effects by neutrons and  $\gamma$ -rays on scintillation light is estimated by calculating the absorption powers due to SXs, neutrons, and  $\gamma$ -rays.

#### 3.1 The absorption power due to SXs

Here, SX emission is assumed to be bremsstrahlung only. Usually an SX is contributed by impurity and recombination radiation as well as bremsstrahlung. The contributions of impurity and recombination radiation are discussed in Sec. 3.4. The power of bremsstrahlung emitted from a unit volume in a plasma is given by Eq. (1) [10] as

$$\omega(\nu) = 6.3 \times 10^{-53} Z_{\text{eff}}^2 \left( \frac{e}{T_e} \right)^{1/2} n_e n_i \exp\left(-\frac{h\nu}{T_e}\right). \quad (1)$$

In Eq. (1),  $Z_{\text{eff}}$  is the effective ion charge,  $n_e$  and  $n_i$  are the electron and ion density respectively,  $T_e$  is the electron temperature,  $e$  is the elementary charge,  $h$  is the Planck constant, and  $\nu$  is the frequency of a photon. With Be foil, low energy photons, which have a lower frequency than  $\nu_0$ , are cut. This  $\nu_0$  is determined by the attenuation rate of Be. Therefore, the incident power to the CsI scintillator from a plasma is estimated by Eq. (2) [11].

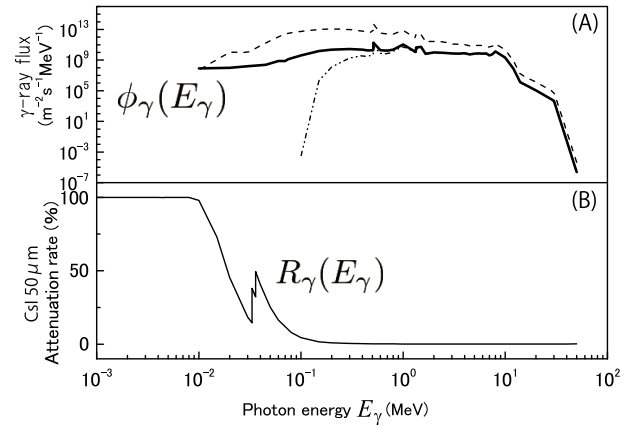


Fig. 3 Figure (A) shows three lines indicating different types of the energy spectrum of the  $\gamma$ -ray flux. The thick solid line shows the  $\gamma$ -ray flux,  $\phi_\gamma$ , calculated by DORT and PHITS. The upper dotted line shows the flux calculated by DORT without  $\gamma$ -ray shielding, and the lower dotted line shows the reduced flux with  $\gamma$ -ray shielding. Figure (B) shows the attenuation rate of CsI [12].

$$W_{\text{SX}} = \int_{l_c} 1.6 \times Z_{\text{eff}}^2 \frac{n_e n_i}{(10^{19})^2} \left( \frac{T_e}{e} \right)^{\frac{1}{2}} \times \exp\left(-\frac{h\nu_0}{T_e}\right) \frac{\Delta\Omega}{4\pi} S_p dl_c. \quad (2)$$

Here,  $\Delta\Omega$  is the solid angle from a plasma to the CsI scintillator.  $S_p$  is the area of the detector, projected in the plasma through the pinhole.  $l_c$  is the length along the sight lines.

The amplitude of  $W_{\text{SX}}$  is contributed mainly by photons whose respective energy is almost the same as the plasma electron temperature. The attenuation rate of CsI, as a function of the photon energy  $E_\gamma$ , is shown in Fig. 3 [12]. In the energy region under 0.1 MeV, photoelectric effect is dominant. Considering the electron temperature of LHD, up to 10 keV, most of the bremsstrahlung is expected to be absorbed by CsI. Therefore, it is appropriate that  $W_{\text{SX}}$  is the absorption power due to SXs.

The plasma is assumed to be quasi-neutral,  $n_e = n_i$  and including only hydrogen,  $Z_{\text{eff}} = 1$ . The electron temperature profile is assumed to be a parabolic one, and the electron density is constant,  $n_e = 2.5 \times 10^{19} \text{ m}^{-3}$ . When the thickness of Be foil is 15  $\mu\text{m}$ , the cut-off energy of the Be foil is  $h\nu_0 = 1.3 \text{ keV}$ .  $\frac{\Delta\Omega}{4\pi} S_p = 3.0 \times 10^{-10} \text{ str m}^2$ , when the size of the pinhole is 2 mm (toroidally)  $\times$  6 mm (radially), the distance between a plasma core and the pinhole is almost 3.9 m, and the distance between the scintillator and the pinhole is 0.6 m. With these parameters, Eq. (2) is evaluated numerically as  $W_{\text{SX}} = 3.49 \times 10^{-7} \text{ W}$  when the central electron temperature is 9.46 keV, and  $W_{\text{SX}} = 2.55 \times 10^{-8} \text{ W}$  when the central electron temperature is 1 keV.

#### 3.2 The absorption power due to $\gamma$ -rays

In the  $\gamma$ -ray case, the absorption power is estimated as

$$W_\gamma = S \int E_\gamma R_\gamma(E_\gamma) \phi_\gamma(E_\gamma) dE_\gamma. \quad (3)$$

This equation shows the process in which  $\gamma$ -rays, as photons, are absorbed by a CsI crystal.  $S$  is the area of the scintillator,  $8 \text{ mm} \times 8 \text{ mm}$ .  $\phi_\gamma$  is the energy spectrum of the  $\gamma$ -ray flux calculated by DORT and PHITS with  $\gamma$ -ray shielding, shown as the thick solid line in Fig. 3 (A).  $R_\gamma(E_\gamma)$ , shown in Fig. 3 (B) is the attenuation rate of CsI.  $R_\gamma(E_\gamma)$  is defined by  $1 - \exp\{-\mu(E_\gamma)l\}$ .  $\mu$  is the attenuation coefficient of CsI [12]. The attenuation coefficient is composed of the cross sections for the photoelectric absorption, coherent scattering, incoherent (Compton) scattering, and electron-positron production in the fields of the nucleus and of the atomic electrons.

In Fig. 3 (A), the upper dotted line shows the flux calculated by DORT without  $\gamma$ -ray shielding. The geometry for the calculation is shown in Fig. 2. However, this geometry does not include stainless steel as  $\gamma$ -ray shielding. The energy spectrum would be changed through the shielding. The lower dotted line shows the changed energy spectrum when the thickness of the shielding is 100 mm. With the shielding, at the same time,  $\gamma$ -rays are produced in the shielding with (n,  $\gamma$ ) reactions or others. The thick solid line shows the sum of the reduced spectrum and the spectrum of produced  $\gamma$ -rays.

In Eq. (3), the attenuation rate is used as the absorption rate of the  $\gamma$ -ray energy. However, usually, the absorption rate should be smaller than the attenuation rate. And the power used for scintillation is due to the absorption power, not the attenuation power. Then the  $W_\gamma$  should be smaller in a practical sense.

With these parameters, Eq. (3) is evaluated numerically as  $W_\gamma = 4.24 \times 10^{-9} \text{ W}$ .

### 3.3 The absorption power due to neutrons

In the neutron case, effect by neutrons which enters directly into a CsI crystal is considered. In particular, the elastic collision process is considered. The absorption power, due to  $\alpha$  particles and protons by (n,  $\alpha$ ) or (n, p) reactions in CsI, is ignored, since the power is small compared with the power due to the elastic collision process from our estimation. The absorption power due to induced  $\gamma$ -rays in CsI by (n,  $\alpha$ ) or (n,  $\gamma$ ) reactions is ignored, since a thin CsI crystal is expected to absorb a small amount of the  $\gamma$ -ray power.

The absorption power due to the elastic collision process is given by Eq. (4).

$$W_n = VN \int \sum_{i=\text{Cs,I}} E_n R_{n,i} \phi_n(E_n) \sigma_i(E_n) dE_n. \quad (4)$$

Here,  $N$  is the density of the atom of Cs or I.  $R_{n,i}$  ( $i = \text{Cs, I}$ ) is the averaged absorption rate of the neutron energy. Then,  $E_n R_{n,i}$  is the energy given to a nucleus by an elastic collision of a neutron and a nucleus.  $R_{n,i}$  is given as  $R_{n,i} = (1 - \alpha_i)/2$  [13].  $\alpha_i$  is the collision parameter of a

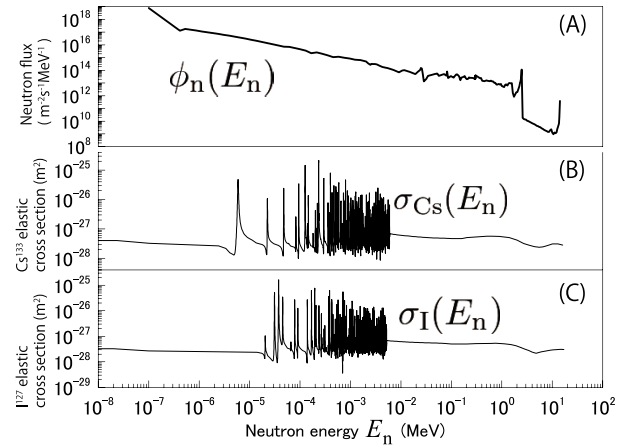


Fig. 4 Figure (A) shows the energy spectrum of the neutron flux,  $\phi_n$ , calculated by DORT. Figures (B) and (C) show the elastic cross sections of  $\text{Cs}^{133}$  and  $\text{I}^{127}$ , respectively [14].

nucleus of Cs or I. This is given as  $\alpha_i = \left(\frac{A_i-1}{A_i+1}\right)^2$ , where  $A_i = \frac{m_i}{m_n}$  ( $i = \text{Cs, I}$ ).  $\phi_n$  shown in Fig. 4 (A) is the energy spectrum of the neutron flux, calculated by DORT. The attenuation of the flux by  $\gamma$ -ray shielding is not considered, since neutrons would enter the space in front the scintillator through the pinhole and fill it by scattering on the surface of the vacuum vessel without significant loss of its energy.  $\sigma_i$  ( $i = \text{Cs, I}$ ), as shown in Figs. 4 (B) and (C), is the elastic cross section of a Cs or I nucleus.  $E_n$  is the neutron energy.

The definition of  $\alpha_i$  shows the energy given to a nucleus by an elastic collision is smaller when the mass number of the nucleus is greater. This is an advantage in using a CsI:TI scintillator in high neutron flux environments.

In Eq. (4), each neutron is expected to collide with a nucleus only once in the CsI scintillator, because if a neutron perpendicularly enters into the area  $S$ , the minimum mean free path is longer than the thickness  $l$ ,  $50 \mu\text{m}$ . And, all the power due to the elastic collision process is assumed to be used to scintillate. Strictly speaking, all of the energy absorbed by nuclei is not used for scintillation. However, the process by which the energy activates electrons is complicated and ignored.

The expression of  $R_n$  is not correct with an elastic collision of a heavy nucleus and a high energy neutron [13]. In that collision case, the value of  $R_n$  is smaller than that given by  $(1 - \alpha_i)/2$ .

Now, we only consider  $\text{Cs}^{133}$  and  $\text{I}^{127}$ , which are the only stable isotopes in nature.  $N = 1.05 \times 10^{28} \text{ m}^{-3}$  with the density of CsI,  $4.51 \text{ g cm}^{-3}$  and the molar formula weight of CsI,  $260 \text{ g mol}^{-1}$ . The data of the elastic cross section is obtained from JENDL-4.0 database [14].  $A_{\text{Cs}^{133}} \sim 133$ , and  $A_{\text{I}^{127}} \sim 127$ , because the mass of a nucleus is similar to the product of the mass number and the mass of a neutron. Therefore,  $R_{n,\text{Cs}^{133}} = 1.48 \times 10^{-2}$ , and  $R_{n,\text{I}^{127}} = 1.55 \times 10^{-2}$ . With these parameters, Eq. (4) is evaluated numerically as  $W_n = 3.58 \times 10^{-9} \text{ W}$ .

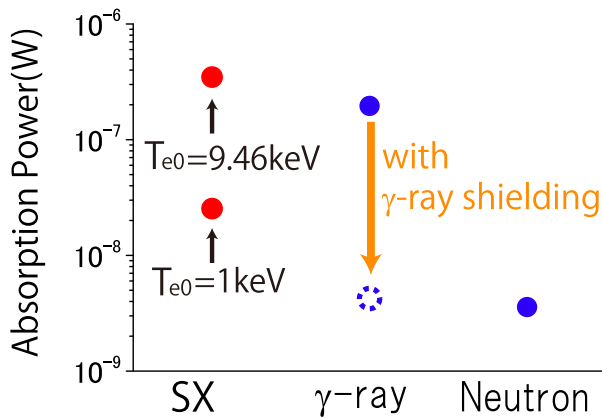


Fig. 5 The absorption powers due to SXs,  $\gamma$ -rays, and neutrons are shown.

### 3.4 A conclusion of estimations

Figure 5 shows the summary of the estimations of the absorption powers. The power due to SXs is at least one order larger than other contributions when the central plasma electron temperature is 1 keV. It is also noted that recombination and impurity radiation contribute to SX emission, as well [15]. Actually, in LHD, absolute measurements of SX emission showed that the amplitude of the SX emission is about 10 times greater than an estimation from Eq. (2) [11]. This means the diagnostic will work well as an SX detector even in the maximum neutron yield discharges.

## 4. Summary

In summary, we have designed a new scintillator-based SX diagnostic usable in LHD deuterium plasma experiments. To estimate effects on scintillation light by radiations, the absorption powers due to SXs,  $\gamma$ -rays, and neutrons are calculated. The result of the estimation shows that setting  $\gamma$ -ray shielding is critical for SX measurements in LHD deuterium plasma experiments. The power due to the SX emission is expected to be at least one factor of 10

larger than that due to neutrons and  $\gamma$ -rays with appropriate  $\gamma$ -ray shielding. We plan to examine a scintillator-based SX diagnostic with deuterium plasmas in the near future.

## Acknowledgements

The authors would like to acknowledge useful comments and suggestions by Prof. M. Isobe, Prof. T. Nishitani, Dr. K. Ogawa, Dr. T. Tanaka (National Institute for Fusion Science), and Prof (Emeritus). M. Sasao.

This work was supported by NIFS budget code ULPP028 and is also partially supported by the Ministry of Education, Science, Sports and Culture, Grant-in-Aid for Scientific Research 26249144, by the JSPS-NRF-NSFC A3 Foresight Program (NSFC: No. 11261140328, NRF: No. 2012K2A2A6000443), and by NIFS/NINS under the project of Formation of International Scientific Base and Network.

- [1] S. Ohdachi *et al.*, *Fusion Sci. Technol.* **58**, 418 (2010).
- [2] Glenn F. Knoll, *Radiation detection and measurement* (4th Edition), (Wiley, 2010) Chap. 8.
- [3] A. Weller, *Nucl. Instrum. Methods Phys. Res. A* **623** (2010).
- [4] S. Ohdachi *et al.*, *Rev. Sci. Instrum.* **74**, 2136 (2003).
- [5] L.F. Delgado-Aparicio *et al.*, *Rev. Sci. Instrum.* **75**, 4020 (2004).
- [6] D. Stutman *et al.*, *Rev. Sci. Instrum.* **76**, 023505 (2005).
- [7] D. Stutman *et al.*, *Rev. Sci. Instrum.* **83**, 10E535 (2012).
- [8] W.A. Rhoades *et al.*, *Nucl. Sci. Eng.* **99**, 88 (1988).
- [9] T. Sato *et al.*, *Nucl. Sci. Eng.* **50**, 9 (2013).
- [10] K. Miyamoto, *Plasma Physics for Nuclear Fusion* (Revised edition), (The MIT Press, 1989) Chap. 15.
- [11] S. Ohdachi, PhD Thesis (Nagoya University) p. 48 (2003).
- [12] M.J. Berger *et al.*, XCOM: Photon Cross Sections Database, U.S. National Institute of Standards and Technology the downloadable version 3.1 (2010).
- [13] J.R. Lamarsh and A.J. Baratta, *Introduction to Nuclear Engineering* (3rd Edition), (Prentice Hall, 2001) Chap. 3.
- [14] K. Shibata *et al.*, *Nucl. Sci. Eng.* **48**, 1 (2011).
- [15] I.H. Hutchinson, *Principles of Plasma Diagnostics* (Cambridge University Press, 2002) Chap. 5.